International Journal of Heat and Mass Transfer 52 (2009) 4545–4552

Contents lists available at ScienceDirect

International Journal of Heat and Mass Transfer

journal homepage: www.elsevier.com/locate/ijhmt

Laminar plane fountains impinging on a ceiling with an opposing heat flux

N. Srinarayana [a,*], S.W. Armfield [a], Wenxian Lin [b]

[a] School of Aerospace, Mechanical and Mechatronic Engineering, The University of Sydney, NSW 2006, Australia
[b] School of Engineering, James Cook University, Townsville, Qld 4811, Australia

ARTICLE INFO

Article history:
Received 13 November 2008
Received in revised form 12 March 2009
Accepted 12 March 2009
Available online 4 May 2009

Keywords:
Impinging plane fountain
Buoyancy dominated flows
Opposing heat flux
Stratification
Numerical simulation
Scaling

ABSTRACT

The behaviour of unsteady planar strong fountains, impinging on a ceiling with an opposing heat flux on the ceiling, is investigated numerically for $8.0 \leqslant Fr \leqslant 30.0$ at $Re = 50$ and $Pr = 7$. The height of the ceiling is varied in $10 \leqslant H/X_{in} \leqslant 25$, where X_{in} is the half-width of the fountain source, and the non-dimensional gradient of the temperature difference between the fountain source and the ceiling is varied for $0.2 \leqslant \Delta\theta/(H/X_{in}) \leqslant 1.8$. It is found that the fountain does not hit the ceiling, but instead stagnates and spreads at some distance from the ceiling due to the stratification of the fluids in the immediate vicinity of the ceiling. The scaling and direct numerical simulation results show that the augmented spreading distance $H_d + X_d$ has the scaling of $H_d + X_d \sim X_{in} Fr^{2/9} (H/X_{in})^{1/2} [\Delta\theta/(H/X_{in})]^{-1/3}$ in the range studied, where H_d is the maximum fountain height, X_d is the spreading distance measured at H_d, respectively.

1. Introduction

Fountains (negatively buoyant jets) occur whenever a fluid is injected upwards into a lighter fluid (or downwards into a denser fluid). Fountains can be broadly classified as free fountains where the jet penetrates a finite distance in the ambient fluid and falls back as a plunging plume around the entering fluid and impinging fountains where the jet impinges on a flat ceiling or any other interface and moves outwards along the interface until gravity forces the intrusion fluid to fall.

Impinging fountains have many engineering applications. A case of particular interest is in heating and ventilation of buildings by downward facing jets located at the ceiling. In this case buoyancy effects combined with heat losses through floors and walls will act to generate stratification. Effective heating and ventilation of the room will depend on the jet momentum and mixing being sufficient to counteract the tendency of the heat losses to produce a stratification and hence accurate prediction of such flows is essential for effective design of such systems. Similar flows are encountered in artificially induced circulation used for de-stratification in reservoirs to improve the water quality by preventing the formation of anoxic bottom water, and discharge of sewage dispersed into marine environment by mixing.

The characteristics of plane fountains are governed by the Froude number, the Reynolds number, and the Prandtl number, defined as,

$$Fr \equiv \frac{V_{in}}{\sqrt{g(\rho_{in} - \rho_\infty)/\rho_\infty X_{in}}} = \frac{V_{in}}{\sqrt{g\beta(T_\infty - T_{in})X_{in}}}, \tag{1}$$

$$Re \equiv \frac{V_{in} X_{in}}{\nu}, \tag{2}$$

$$Pr \equiv \frac{\nu}{\kappa}, \tag{3}$$

where X_{in} is the half-width of the inlet jet. The second expression of the Froude number applies when the density difference is due to the difference in temperature of the fountain and the ambient fluids using the Oberbeck–Boussinesq approximation. For impinging fountains with opposing buoyancy, additional control parameters are H, the height of the ceiling, and $\Delta\theta$, the temperature gradient between the fountain source and the ceiling. Alternatively, the Richardson number, $Ri = 1/Fr^2$, has also been used in some studies (see, e.g., [1–3]).

There have been significant studies on both free fountains and fountains impinging on a solid boundary or a density interface in both round and planar configurations. Most early studies focussed on turbulent fountains [4–16]. More recently, laminar ($Re \lesssim 200$) and weak ($Fr \lesssim 1.0$) fountains have also received significant attention due to their fundamental and application significance [17–22]. Friedman et al. [3] studied the onset of instability in fountains and obtained the critical Froude number for transition from a steady to an unsteady fountain as $Fr = 2.0$ and $Fr = \sqrt{2}$ for fountains with uniform and parabolic inlet velocity profiles at the fountain source, respectively. In a similar study, Srinarayana et al. [23] obtained the critical Froude number for unsteadiness as $Fr = 2.25$ with uniform inlet velocity profile at the fountain source. Williamson et al. [24]

* Corresponding author. Tel.: +61 2 9351 7140; fax: +61 2 9351 7060.
E-mail address: snag3258@mail.usyd.edu.au (N. Srinarayana).

0017-9310/$ - see front matter © 2009 Elsevier Ltd. All rights reserved.
doi:10.1016/j.ijheatmasstransfer.2009.03.015

Nomenclature

b	buoyancy flux per unit mass per unit span
Fr	Froude number
g	acceleration due to gravity
H	height of the ceiling
H_d	maximum fountain penetration height
m	momentum flux per unit mass per unit span
P	dimensional pressure
p	non-dimensional pressure
Pr	Prandtl number
R	radius
Re	Reynolds number
s	non-dimensional temperature stratification number
T	dimensional temperature of fluid
U	dimensional horizontal velocity
u	non-dimensional horizontal velocity
V	dimensional vertical velocity
v	non-dimensional vertical velocity
X	dimensional horizontal coordinate
X_d	spreading distance
x	non-dimensional horizontal coordinate
Y	dimensional vertical coordinate
y	non-dimensional vertical coordinate
Z_m	dimensional fountain height
z_m	non-dimensional fountain height

Greek symbols

β	coefficient of volumetric expansion
κ	thermal diffusivity
ν	kinematic viscosity
ρ	fluid density
τ	non-dimensional time
θ	non-dimensional temperature of fluid
$\Delta\theta$	non-dimensional temperature difference between fountain source and ceiling

Subscripts

in	variable index at source
∞	variable index of ambient

conducted a series of experiments on round fountains and classified different fountain behaviour on a Re—Fr plane and obtained the critical Reynolds number for transition from a laminar to a turbulent flow as $Re \sim 120$.

There have been no detailed studies on impinging fountains opposed by a stratification generated by an opposing buoyancy flux on the upper boundary. However, fountains in a stratified fluid, a configuration that closely approximates such flows, have been studied in the past. Bloomfield and Kerr [25,26] conducted both theoretical and experimental investigations into the behaviour of turbulent fountains in a confined stratified environment and showed that the fountain would form an initial front at an intermediate height that would continue to rise and ultimately impinge on the far boundary, completely purging the domain. Lin and Armfield [27] studied the behaviour of weak axisymmetric and planar fountains resulting from the injection of denser fluid upwards into large containers containing stably stratified fluid using scaling and numerical analysis. They obtained the following scaling for the non-dimensional maximum fountain penetration height z_m,

$$z_m = \frac{Z_m}{X_{in}} \sim \frac{Fr^{2/3}}{Re^{1/3}s^{1/3}}, \tag{4}$$

where $s = d\theta_\infty/dy$ is the non-dimensional temperature stratification number, and validated this relation with direct numerical simulation results for $0.2 \leqslant Fr \leqslant 1.0$, $20 \leqslant Re \leqslant 200$ and $0.1 \leqslant s \leqslant 5.0$. There have been many other numerical investigations on impinging jets. Some of which are summarised in [28–32]. Other studies on fountains interacting with a density interface can be found in [33,34].

In the current paper, the behaviour of two-dimensional impinging plane fountains formed by jets injected vertically upwards into a homogeneous fluid of lower density with opposing buoyancy is investigated for $8.0 \leqslant Fr \leqslant 30.0$, $10 \leqslant H/X_{in} \leqslant 25$ and $0.2 \leqslant \Delta\theta/(H/X_{in}) \leqslant 1.8$ at constant Reynolds and Prandtl numbers of $Re = 50$ and $Pr = 7$. In this case the buoyancy effects are a result of the temperature variation between the fountain, the ambient and the ceiling. The scaling for the augmented spreading distance is presented in Section 2. The configuration and solver are briefly introduced in Section 3. The time evolution and the flow characteristics of the impinging fountain and the numerical validation of the scaling are presented in Section 4, followed by the conclusions in Section 5.

2. Scaling

The system configuration and typical flow characteristics of the impinging plane fountains under consideration are illustrated in Fig. 1. The fluid between a horizontal insulated solid wall at the bottom and another solid wall at a temperature T_w at the ceiling, distance H apart, is initially still and isothermal at a temperature T_∞. For $t \geqslant 0$ a jet of fluid issues from a slot of width $2X_{in}$ on the floor with a uniform velocity V_{in} and a temperature $T_{in} < T_\infty$. The flow is assumed to remain two-dimensional. The initial buoyancy experienced by the fountain until it impinges on the ceiling is a result of the temperature difference between the source fluid and the ambient fluid. After that, the stratification of the fluids in the immediate vicinity of the ceiling due to the temperature difference between the ambient fluid and T_w at the ceiling will influence the subsequent fountain flow behaviour, as evidenced by the fact that the fountain will not directly contact the ceiling, but instead stagnates and spreads a distance X_d at some distance from the ceiling (at the height H_d) before it falls. However, in the absence of any ceiling the fountain would attain its maximum height Z_m which is equivalent to $(X_d + H_d)$ in the current analysis and it is appropriate that the scaling be based on this augmented spreading distance rather than H_d alone.

As the Reynolds number and the Prandtl number are kept constant in this study, the scale for the augmented spreading distance $H_d + X_d$ can be assumed to be expressed in terms of the powers of the momentum flux m_{in}, the buoyancy flux b_{in}, the height of the ceiling H, and $\Delta\theta/H$ as follow,

$$H_d + X_d \sim m_{in}^{\alpha} b_{in}^{\beta} H^{\phi} \left(\frac{\Delta\theta}{H}\right)^{\zeta}, \tag{5}$$

where $\Delta\theta = (T_w - T_{in})/(T_\infty - T_{in})$ is the non-dimensional temperature difference between that at the fountain source and that at the ceiling, and α, β, ϕ, and ζ are the powers for the corresponding parameters, which can be determined using dimensional analysis.

The dimensional analysis gives the following scaling for the augmented spreading distance $H_d + X_d$,

$$H_d + X_d \sim X_{in} Fr^{\frac{4}{3}(1-\phi+\zeta)} \left(\frac{H}{X_{in}}\right)^{\phi} \left(\frac{\Delta\theta}{H/X_{in}}\right)^{\zeta}. \tag{6}$$

In non-dimensional form, this scaling becomes,

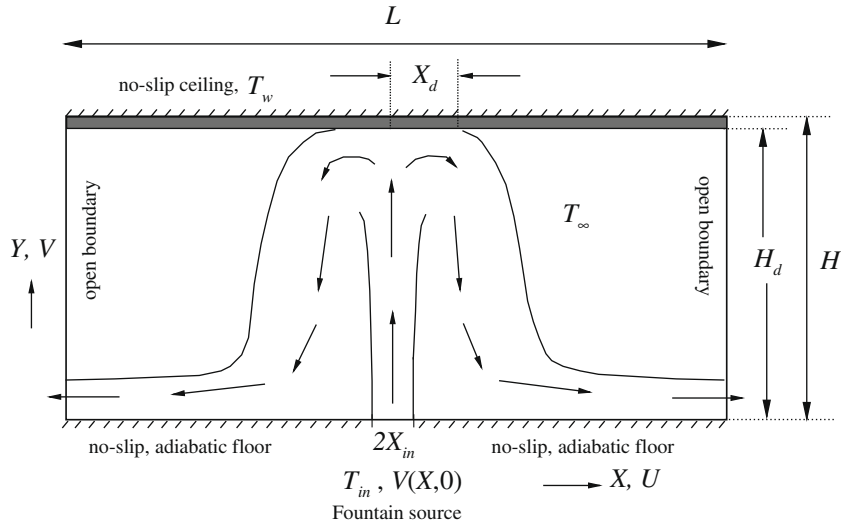

Fig. 1. Configuration of the system and the computational domain.

$$\frac{H_d + X_d}{X_{in}} \sim Fr^{\frac{4}{3}(1-\phi+\zeta)} \left(\frac{H}{X_{in}}\right)^{\phi} \left(\frac{\Delta\theta}{H/X_{in}}\right)^{\zeta}. \tag{7}$$

If the height of the ceiling is large enough such that the fountain does not impinge (free fountain), $H_d + X_d \sim Z_m$ with $\phi = 0$ and the fountain is also independent of $\Delta\theta/H$, such that,

$$z_m = \frac{Z_m}{X_{in}} \sim Fr^{\frac{4}{3}}, \tag{8}$$

which is exactly the same as the scaling obtained by Baines et al. [6] for turbulent plane fountains. However in the present case, the powers ϕ and ζ are unknown and will be evaluated empirically. There is no previous analytical scaling, obtained from dimensional analysis, available in the literature.

3. Numerical model

The governing equations are the incompressible Navier–Stokes equations with the Oberbeck–Boussinesq approximation for buoyancy and the temperature equation. These equations can be written in the conservative, non-dimensional form in Cartesian coordinates as follows,

$$\frac{\partial u}{\partial x} + \frac{\partial v}{\partial y} = 0, \tag{9}$$

$$\frac{\partial u}{\partial \tau} + \frac{\partial (uu)}{\partial x} + \frac{\partial (vu)}{\partial y} = -\frac{\partial p}{\partial x} + \frac{1}{Re}\left(\frac{\partial^2 u}{\partial x^2} + \frac{\partial^2 u}{\partial y^2}\right), \tag{10}$$

$$\frac{\partial v}{\partial \tau} + \frac{\partial (uv)}{\partial x} + \frac{\partial (vv)}{\partial y} = -\frac{\partial p}{\partial y} + \frac{1}{Re}\left(\frac{\partial^2 v}{\partial x^2} + \frac{\partial^2 v}{\partial y^2}\right) + \frac{1}{Fr^2}\theta, \tag{11}$$

$$\frac{\partial \theta}{\partial \tau} + \frac{\partial (u\theta)}{\partial x} + \frac{\partial (v\theta)}{\partial y} = \frac{1}{RePr}\left(\frac{\partial^2 \theta}{\partial x^2} + \frac{\partial^2 \theta}{\partial y^2}\right). \tag{12}$$

The following non-dimensionalisation is used for the parameters in the equations:

$$x = \frac{X}{X_{in}}, \quad y = \frac{Y}{X_{in}}, \quad u = \frac{U}{V_{in}}, \quad v = \frac{V}{V_{in}},$$
$$\tau = \frac{t}{(X_{in}/V_{in})}, \quad p = \frac{P}{\rho V_{in}^2}, \quad \theta = \frac{T - T_\infty}{T_\infty - T_{in}}. \tag{13}$$

As illustrated in Fig. 1, the initial and boundary conditions are,

$$u = v = \theta = 0 \quad \text{when} \quad \tau < 0, \tag{14}$$

and open boundaries at left and right edges:

$$\frac{\partial u}{\partial x} = 0, \quad \frac{\partial v}{\partial x} = 0, \quad \frac{\partial \theta}{\partial x} = 0 \quad \text{on} \quad x = \pm L/(2X_{in}), \quad \forall y \tag{15}$$

isothermal uniform velocity at inlet:

$$u = 0, \quad v = 1, \quad \theta = -1 \quad \text{on} \quad |x| \leqslant 1, \quad y = 0, \tag{16}$$

no-slip adiabatic floor:

$$u = v = 0, \quad \frac{\partial \theta}{\partial y} = 0 \quad \text{on} \quad |x| > 1, \quad y = 0, \tag{17}$$

no-slip isothermal ceiling:

$$u = v = 0, \quad \theta = \theta_w \quad \forall x, \quad y = H/X_{in}, \tag{18}$$

respectively. It is assumed that the variation of flow variables in the boundary normal direction at the left and the right open boundaries is negligible. Further, it is ensured that the open boundaries are sufficiently far from the region of interest.

The results are obtained using *Gerris* [23,35], an open source quad-tree based adaptive mesh solver which uses a fractional-step projection method. The total length of the computational domain is $L = 300X_{in}$, i.e., $-150 \leqslant x \leqslant +150$, and the height H is varied so that the fountain impinges on the ceiling. A typical adapted mesh is shown in Fig. 2 for $Fr = 10.0$, $H/X_{in} = 25$ and $\Delta\theta/(H/X_{in}) = 0.8$. The adaptive meshing is observed for both the fountain and the stratified fluid layer. The resulting adapted mesh at full development, for the example shown in Fig. 2, has 341369 cells with a time-step of 4.33×10^{-4} and a run time of the order of 72 h on a typical 3.2 GHz Pentium-IV machine with 1 GB RAM.

4. Results

All the results are obtained at a fixed Reynolds number of $Re = 50$ and Prandtl number of $Pr = 7$. An overview of the temperature field evolution for a typical fountain impinging on a ceiling with opposing buoyancy is shown in Fig. 3 for $Fr = 20.0$, $H/X_{in} = 25$ and $\Delta\theta/(H/X_{in}) = 0.8$. After initiation, the fountain travels upwards. The fountain advances more slowly with time and the width of the head increases, as can be seen in Fig. 3a–c. The increase in thickness of the stratified fluid layer due to conduction

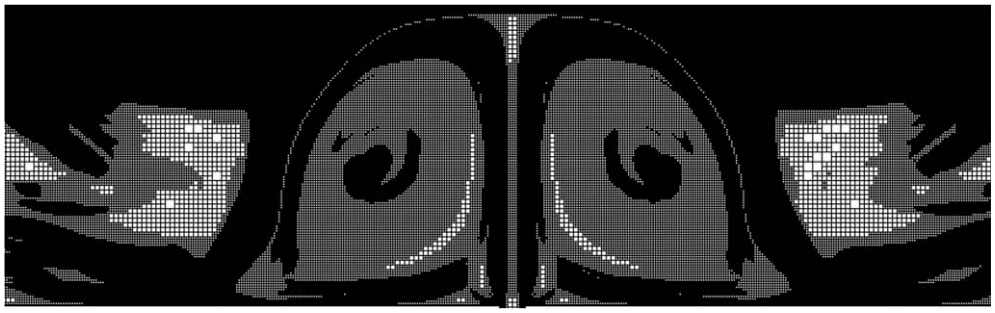

Fig. 2. A typical adapted mesh.

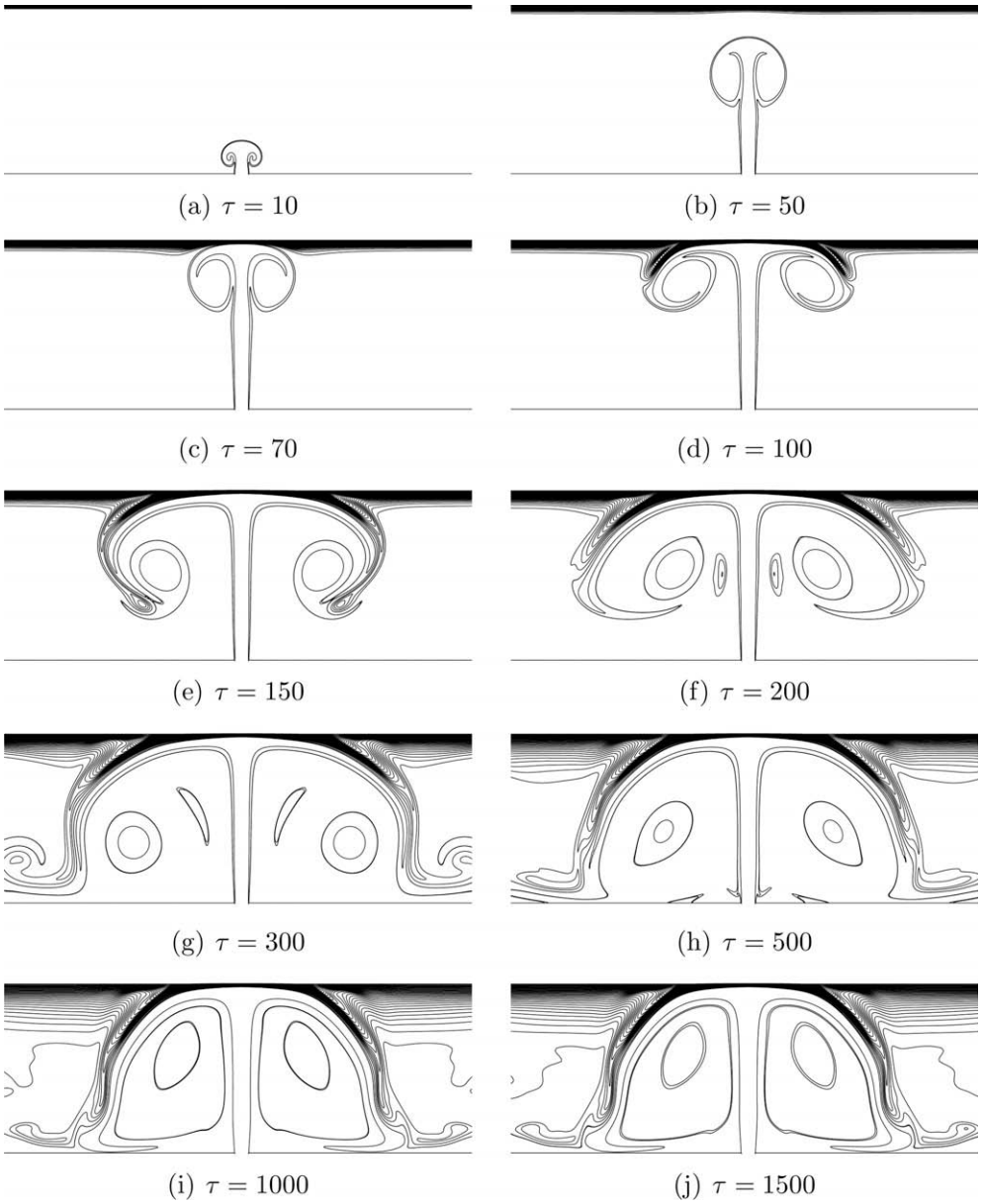

Fig. 3. Time evolution of temperature fields for a typical impinging fountain with opposing buoyancy at $Fr = 20.0$, $H/X_{in} = 25$ and $\Delta\theta/(H/X_{in}) = 0.8$, with contour interval $\Delta\theta = 0.5$.

from the ceiling is also observed in Fig. 3. In Fig. 3c, the fountain is seen to impinge and perturb this stratified fluid layer. At some stage the fountain rise is halted completely and it then stagnates with the stagnation pressure causing the fluid to spread outwards, as seen in Fig. 3d. The fountain fluid spreads until the buoyancy forces the fluid to fall downwards. Some of the falling fluid is re-en-

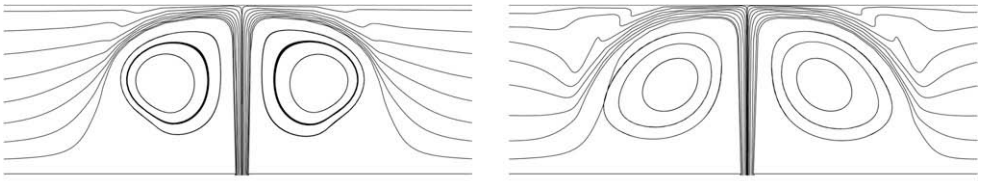

Fig. 4. Streamlines at $Fr = 20.0$, $H/X_{in} = 25$ and $\Delta\theta/(H/X_{in}) = 0.8$.

trained back into the upwards moving fountain core, as seen in Fig. 3e and f and the rest falls down and moves along the floor as a gravity current. This re-entrainment behaviour is further demonstrated by the streamline plots in Fig. 4 at $\tau = 150$ and 200 which show a recirculation region on either side of the fountain core. The fountain is completely symmetric during the time evolution.

Fig. 5 shows the temperature fields for different Fr at $H/X_{in} = 25$ and $\Delta\theta/(H/X_{in}) = 0.8$ at full development. A general increase in the spreading distance with Fr can be seen. The upper impinging region of the fountain is symmetric for these Froude numbers. Fluid from the stratified region is seen to be entrained and carried down by the fountain, with this effect increasing with increasing Fr.

Fig. 6 shows the temperature fields for different $\Delta\theta/(H/X_{in})$ at $Fr = 10.0$ and $H/X_{in} = 25$ at full development. In this case, the spreading distance is seen to decrease with increasing $\Delta\theta/(H/X_{in})$, which is as expected due to increase in the opposing buoyancy. The fountain also penetrates the stratified layer to a lesser extent with increasing $\Delta\theta/(H/X_{in})$.

In Fig. 7 the temperature fields for varying height of the ceiling at $Fr = 10.0$ and $\Delta\theta/(H/X_{in}) = 0.8$ are shown at full development. A general decrease in the spreading distance with increase in H/X_{in} is observed. Fig. 7 also shows a change in the intrusion behaviour with increasing height of the ceiling. The intrusion rises and penetrates the stratified fluid layer to some extent for $H/X_{in} = 10$, 15 and 17.5, as seen in Fig. 7a–c. This behaviour is absent for higher H/X_{in}.

In the present case, since the ceiling is maintained at a constant temperature for each simulation, fluid at the fountain temperature does not contact the ceiling. Instead fluid at the fountain temperature spreads at some distance from the ceiling due to the stratification of the ambient fluid in the immediate vicinity of the ceiling. The spreading distance is measured on a horizontal line, which is at a distance of 10% of H from the ceiling such that H_d is 90% of H and the spreading distance X_d is the distance from the centreline to the location where the local temperature excess $(T - T_\infty)$ drops to 90% of the inlet excess $(T_{in} - T_\infty)$ on this line.

4.1. $\Delta\theta/(H/X_{in})$ dependence

Fig. 8 shows the variation of non-dimensional augmented spreading distance with $\Delta\theta/(H/X_{in})$ for $0.2 \leqslant \Delta\theta/(H/X_{in}) \leqslant 1.8$ at $Fr = 10.0$ and $H/X_{in} = 25$. In a previous study, Lin and Armfield [27] found that the non-dimensional fountain height, $z_m \sim s^{-1/3}$, where $s = d\theta_\infty/dy$ is the non-dimensional temperature stratification number. In the present situation, the non-dimensional temperature stratification number is taken as equivalent to the variation of the non-dimensional temperature over the domain height, that is, $s \equiv \Delta\theta/(H/X_{in})$ and hence a similar scaling relation

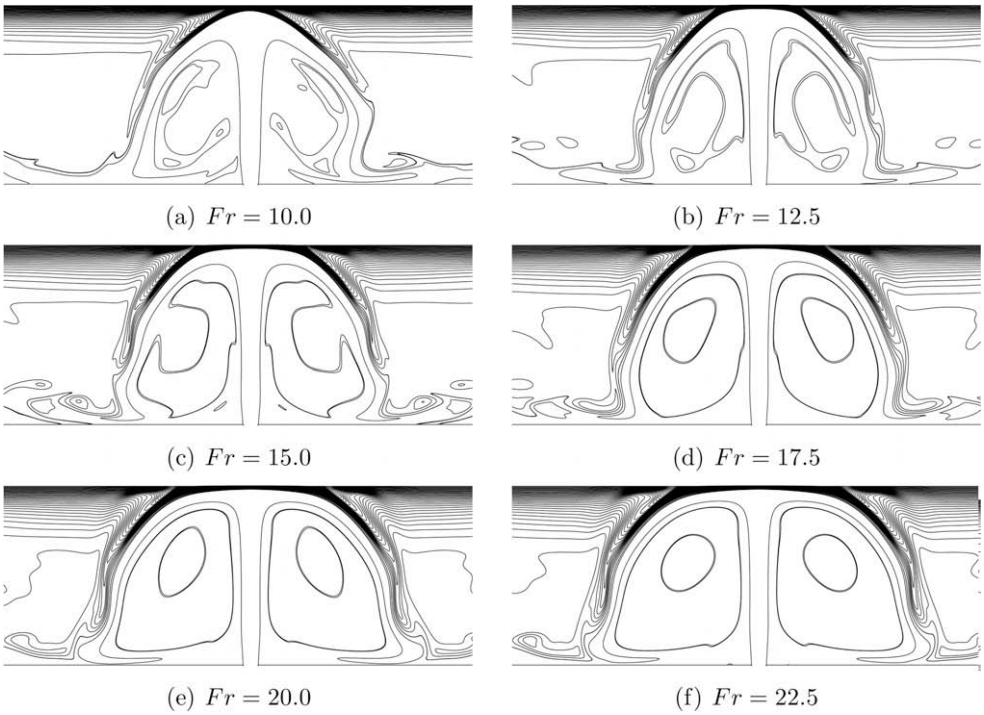

Fig. 5. Temperature fields for different Fr with $H/X_{in} = 25$ and $\Delta\theta/(H/X_{in}) = 0.8$ at full development, with contour interval $\Delta\theta = 0.5$.

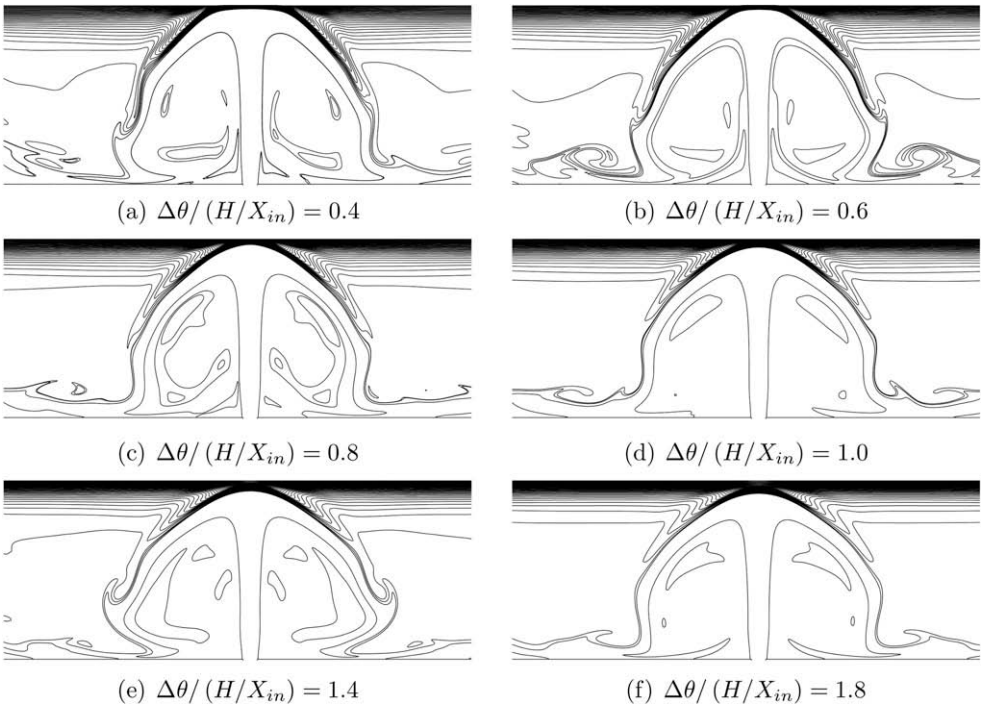

Fig. 6. Temperature fields for different $\Delta\theta/(H/X_{in})$ at $Fr = 10.0$ and $H/X_{in} = 25$ at full development, with contour interval $\Delta\theta = 0.5$.

is tried here. As shown in Fig. 8, $\Delta\theta/(H/X_{in})^{-1/3}$ provides a good fit to the data and the scaling equation is,

$$\frac{H_d + X_d}{X_{in}} \equiv 19.6 + 7.69\left(\frac{\Delta\theta}{H/X_{in}}\right)^{-1/3}, \tag{19}$$

with a variation of less than ± 0.03; $\zeta = -1/3$ is therefore suitable in Eq. (7).

4.2. H/X_{in} dependence

Fig. 9 shows the variation of non-dimensional augmented spreading distance with H/X_{in} for $10 \leqslant H/X_{in} \leqslant 25$ at $Fr = 10.0$ and $\Delta\theta/(H/X_{in}) = 0.8$. It was shown earlier by Holstein and Lemckert [36] and Lemckert [37] that for round fountains impinging on an insulated ceiling, the non-dimensional augmented spreading distance $\sim (H/R_{in})^{1/2}$, where R_{in} is the radius of the nozzle. Similar scaling is tried here and is seen to provide a good fit to the data in Fig. 9, and the scaling equation is,

$$\frac{H_d + X_d}{X_{in}} \equiv -12.5 + 7.9\left(\frac{H}{X_{in}}\right)^{1/2}, \tag{20}$$

with a variation of less than ± 0.04; $\phi = 1/2$ is therefore suitable in Eq. (7).

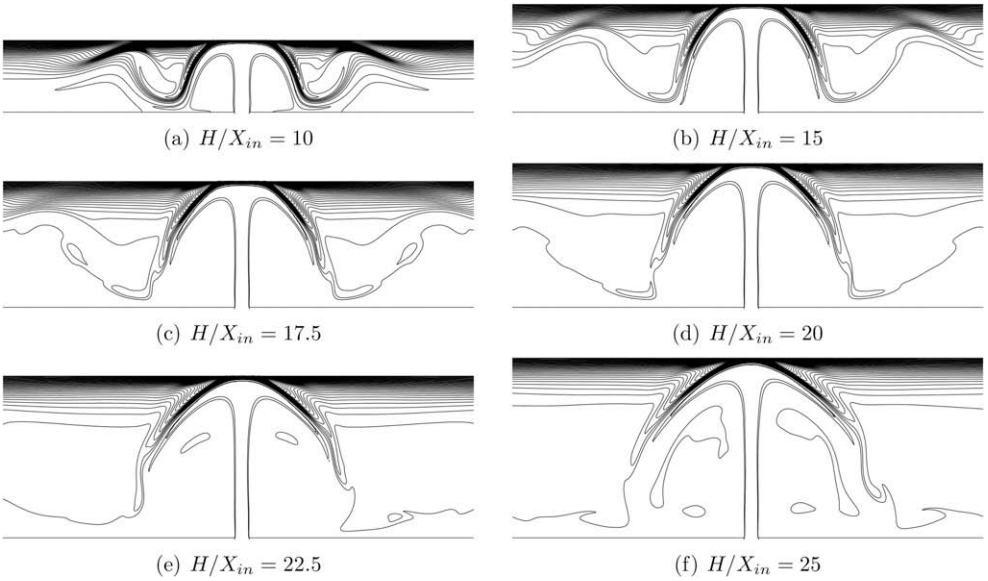

Fig. 7. Temperature fields for different H/X_{in} at $Fr = 10.0$ and $\Delta\theta/(H/X_{in}) = 0.8$ at full development, with contour interval $\Delta\theta = 0.5$.

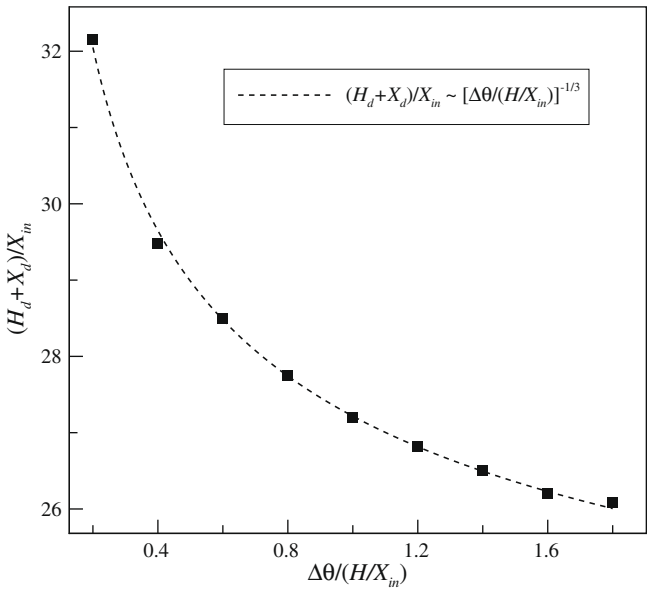

Fig. 8. Variation of the augmented spreading distance with $\Delta\theta/(H/X_{in})$ at $Fr = 10.0$ and $H/X_{in} = 25$.

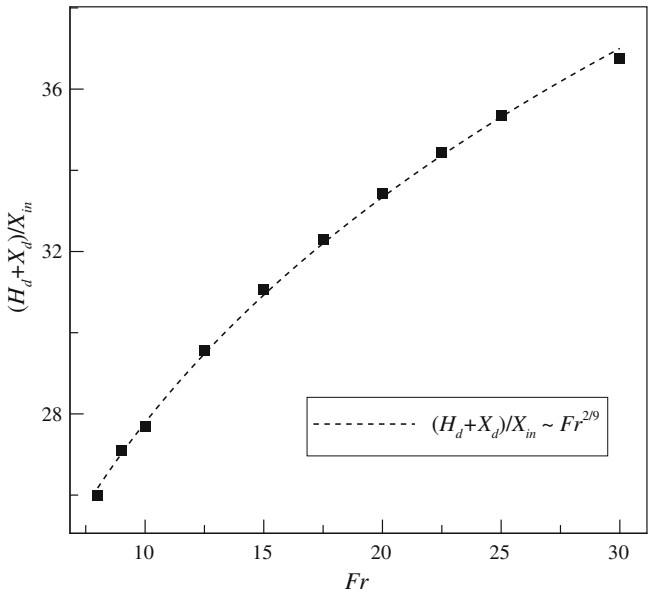

Fig. 10. Variation of the augmented spreading distance with Fr at $H/X_{in} = 25$ and $\Delta\theta/(H/X_{in}) = 0.8$.

4.3. Fr dependence

Fig. 10 shows the variation of non-dimensional augmented spreading distance with Fr for $8.0 \leqslant Fr \leqslant 30.0$ at $H/X_{in} = 25$ and $\Delta\theta/(H/X_{in}) = 0.8$. Since the values of the power indices ϕ and ζ in Eq. (7) are now 1/2 and −1/3, respectively, the scaling equation for constant H/X_{in} and $\Delta\theta/(H/X_{in})$ reduces to,

$$\frac{H_d + X_d}{X_{in}} \sim Fr^{2/9}. \tag{21}$$

Fig. 10 shows that $Fr^{2/9}$ provides a good fit to the data in the range of Fr considered and the scaling equation is,

$$\frac{H_d + X_d}{X_{in}} \equiv -6.3 + 20.4Fr^{2/9}, \tag{22}$$

with a variation of less than ±0.03.

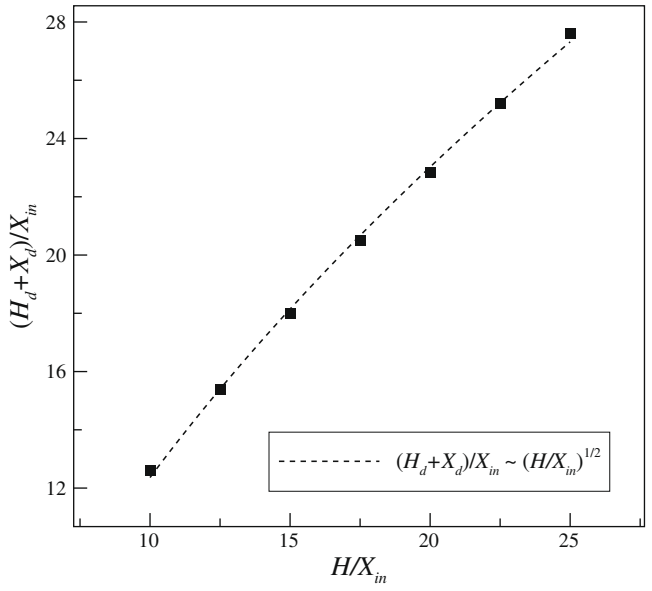

Fig. 9. Variation of the augmented spreading distance with H/X_{in} at $Fr = 10.0$ and $\Delta\theta/(H/X_{in}) = 0.8$.

5. Conclusions

In this paper, the transient behaviour of strong fountains impinging on a ceiling with opposing buoyancy flux is investigated, for $8.0 \leqslant Fr \leqslant 30.0$, $10 \leqslant H/X_{in} \leqslant 25$ and $0.2 \leqslant \Delta\theta/(H/X_{in}) \leqslant 1.8$, using dimensional and numerical analysis. Fountains with uniform inlet velocity profiles at the fountains source are considered.

A scaling was obtained for the augmented spreading distance $H_d + X_d$ by dimensional analysis based on the momentum flux per unit mass per unit span, m_{in}, the buoyancy flux per unit mass per unit span, b_{in}, the height of ceiling H and the non-dimensional temperature difference between the fountain source and the ceiling, which shows that $(H_d+X_d)/X_{in} \sim Fr^{\frac{4}{3}(1-\phi+\zeta)}(H/X_{in})^{\phi}[\Delta\theta/(H/X_{in})]^{\zeta}$, where the power indices ϕ and ζ were obtained numerically.

Numerical simulations were carried out at a fixed Reynolds number of $Re = 50$ and Prandtl number of $Pr = 7$. Initially, qualitative observations were conducted with visualisation of a typical time evolution of numerically simulated transient temperature fields of fountains for varying Fr, H/X_{in} and $\Delta\theta/(H/X_{in})$, to provide an overview of the evolution of the fountains. The augmented spreading distance, $H_d + X_d$, was then obtained at a distance of 10% of H/X_{in} from the ceiling. Quantitative analysis showed that $(H_d + X_d)/X_{in} \sim Fr^{2/9}(H/X_{in})^{1/2}[\Delta\theta/(H/X_{in})]^{-1/3}$ in the range studied, which supported the analytical scaling.

Acknowledgements

The authors acknowledge the support of the Australian Research Council. W. Lin also gratefully acknowledges the support by the National Basic Research Program of China and the National Natural Science Foundation of China.

References

[1] P.D. Friedman, J. Katz, Rise height for negatively buoyant fountains and depth of penetration for negatively buoyant jets impinging an interface, ASME J. Fluid Eng. 122 (2000) 779–782.
[2] P.D. Friedman, Oscillation in height of a negatively buoyant jet, J. Fluid Eng. 128 (2006) 880–882.
[3] P.D. Friedman, V.D. Vadakoot, W.J. Meyer Jr., S. Carey, Instability threshold of a negatively buoyant fountain, Exp. Fluid 42 (2007) 751–759.

[4] J.S. Turner, Jets and plumes with negative or reversing buoyancy, J. Fluid Mech. 26 (1966) 779–792.
[5] I.H. Campbell, J.S. Turner, Fountains in magma chambers, J. Petrol. 30 (1989) 885–923.
[6] W.D. Baines, J.S. Turner, I.H. Campbell, Turbulent fountains in an open chamber, J. Fluid Mech. 212 (1990) 557–592.
[7] B.R. Morton, Forced plumes, J. Fluid Mech. 5 (1959) 151–163.
[8] G. Abraham, Jets with negative buoyancy in homogeneous fluid, J. Hydraul. Res. 5 (1967) 235–248.
[9] T. Mizushina, F. Ogino, H. Takeuchi, H. Ikawa, An experimental study of vertical turbulent jet with negative buoyancy, Warme Stoffubertrag. 16 (1982) 15–21.
[10] H. Zhang, R.E. Baddour, Maximum penetration of vertical round dense jets at small and large Froude numbers, J. Hydraul. Eng. 124 (1998) 550–553.
[11] H. Zhang, R.E. Baddour, Maximum vertical penetration of plane turbulent negatively buoyant jets, J. Eng. Mech. 123 (1997) 973–977.
[12] D. Goldman, Y. Jaluria, Effect of opposing buoyancy on the flow in free and wall jets, J. Fluid Mech. 166 (1986) 41–56.
[13] R.A. Seban, M.M. Behnia, K.E. Abreau, Temperature in a heated air jet discharged downward, Int. J. Heat Mass Transfer 21 (1978) 1453–1458.
[14] L.J. Bloomfield, R.C. Kerr, A theoretical model of a turbulent fountain, J. Fluid Mech. 424 (2000) 197–216.
[15] R.A. Seban, M.M. Behnia, Turbulent buoyant jets in unstratified surroundings, Int. J. Heat Mass Transfer 19 (1976) 1176–1204.
[16] R.W. Cresswell, R.T. Szczepura, Experimental investigation into a turbulent jet with negative buoyancy, Phys. Fluid 5 (1993) 2865–2878.
[17] N.B. Kaye, G.R. Hunt, Weak fountains, J. Fluid Mech. 558 (2006) 319–328.
[18] W. Lin, S.W. Armfield, Very weak fountains in a homogeneous fluid, Numer. Heat Transfer 38 (2000) 377–396.
[19] W. Lin, S.W. Armfield, Direct simulation of weak axisymmetric fountains in a homogeneous fluid, J. Fluid Mech. 403 (2000) 67–88.
[20] P. Philippe, C. Raufaste, P. Kurowski, P. Petitjeans, Penetration of a negatively buoyant jet in a miscible liquid, Phys. Fluid 17 (2005). Art. no. 05360.
[21] W. Lin, S.W. Armfield, Direct simulation of weak laminar plane fountains in a homogeneous fluid, Int. J. Heat Mass Transfer 43 (2000) 3013–3026.
[22] S. Satyanarayana, Y. Jaluria, A study of laminar buoyant jets discharged at an inclination to the vertical buoyancy force, Int. J. Heat Mass Transfer 25 (1982) 1569–1577.
[23] N. Srinarayana, G.D. McBain, S.W. Armfield, W.X. Lin, Height and stability of laminar plane fountains in a homogeneous fluid, Int. J. Heat Mass Transfer 51 (2008) 4717–4727.
[24] N. Williamson, N. Srinarayana, S.W. Armfield, G. McBain, W. Lin, Low Reynolds number fountain behaviour, J. Fluid Mech. 608 (2008) 297–317.
[25] L.J. Bloomfield, R.C. Kerr, Turbulent fountains in a stratified fluid, J. Fluid Mech. 358 (1998) 335–356.
[26] L.J. Bloomfield, R.C. Kerr, Turbulent fountains in a confined stratified environment, J. Fluid Mech. 389 (1999) 27–54.
[27] W. Lin, S.W. Armfield, Weak fountains in a stratified fluid, Phys. Rev. E 66 (2002) 066308.1–066308.10.
[28] J.E. Jaramillo, C.D. Perez-Segarra, I. Rodriguez, A. Oliva, Numerical study of plane and round impinging jets using RANS models, Numer. Heat Transfer B: Fund. 54 (2008) 213–237.
[29] H.M. Hofmann, R. Kaiser, M. Kind, H. Martin, Calculations of steady and pulsating impinging jets – an assessment of 13 widely used turbulence models, Numer. Heat Transfer B: Fund. 51 (2007) 565–583.
[30] L.B.Y. Aldabbagh, I. Sezai, Numerical simulation of three-dimensional laminar, square twin-jet impingement on a flat plate, flow structure, and heat transfer, Numer. Heat Transfer A: Appl. 41 (2002) 835–850.
[31] H. Fujimoto, H. Takuda, N. Hatta, R. Viskanta, Numerical simulation of transient cooling of a hot solid by an impinging free surface jet, Numer. Heat Transfer A: Appl. 38 (1999) 767–780.
[32] M.M. Rahman, A.J. Bula, J.E. Leland, Conjugate heat transfer during free jet impingement of a high Prandtl number fluid, Numer. Heat Transfer B: Fund. 36 (1999) 139–162.
[33] C.Y. Ching, H.J.S. Fernando, Y. Noh, Interaction of a negatively buoyant line plume with a density interface, Dyn. Atmos. Oceans 19 (1993) 367–388.
[34] Y.J.P. Lin, P.F. Linden, The entrainment due to a turbulent fountain at a density interface, J. Fluid Mech. 542 (2005) 25–52.
[35] S. Popinet, Gerris: a tree-based adaptive solver for the incompressible Euler equations in complex geometries, J. Comput. Phys. 190 (2003) 572–600.
[36] D.M. Holstein, C.J. Lemckert, Spreading of energetic submerged fountains impinging on a rigid surface, in: Proceedings of the 14th Australasian Fluid Mechanical Conference, 2001, pp. 749–752.
[37] C.J. Lemckert, Submerged fountains impinging on a smooth horizontal surface, in: Proceedings of the Eighth Australasian Heat and Mass Transfer Conference, 2005.